Acta Biomaterialia 8 (2012) 836–842

Contents lists available at SciVerse ScienceDirect

Acta Biomaterialia

journal homepage: www.elsevier.com/locate/actabiomat

Remineralization of artificial dentinal caries lesions by biomimetically modified mineral trioxide aggregate

Yi-pin Qi [a,1], Nan Li [b,1], Li-na Niu [c], Carolyn M. Primus [d], Jun-Qi Ling [a,*], David H. Pashley [e], Franklin R. Tay [e,*]

[a] Guanghua School of Stomatology, Sun Yat-sen University, Guangzhou, China
[b] College of Osteopedics & Traumatology, Fujian University of Traditional Chinese Medicine, Fuzhou, China
[c] Department of Prosthodontics, School of Stomatology, Fourth Military Medical University, Xi'an, China
[d] Primus Consulting, 7046 Owl's Nest Terrace, Bradenton, FL, USA
[e] School of Graduate Studies, Georgia Health Sciences University, Augusta, GA, USA

ARTICLE INFO

Article history:
Received 3 August 2011
Received in revised form 23 September 2011
Accepted 26 October 2011
Available online 31 October 2011

Keywords:
Biomimetics
Caries
Micro-computed tomography
Mineral trioxide aggregate
Tubular occlusion

ABSTRACT

Fluoride-releasing restorative materials are available for remineralization of enamel and root caries. However, remineralization of dentin is more difficult than remineralization of enamel due to the paucity of apatite seed crystallites along the lesion surface for heterogeneous crystal growth. Extracellular matrix proteins play critical roles in controlling apatite nucleation/growth in collagenous tissues. This study examined the remineralization efficacy of mineral trioxide aggregate (MTA) in phosphate-containing simulated body fluid (SBF) by incorporating polyacrylic acid and sodium tripolyphosphate as biomimetic analogs of matrix proteins for remineralizing caries-like dentin. Artificial caries-like dentin lesions incubated in SBF were remineralized over a 6 week period using MTA alone or MTA containing biomimetic analogs in the absence or presence of dentin adhesive application. Lesion depths and integrated mineral loss were monitored with microcomputed tomography. The ultrastructure of baseline and remineralized lesions was examined by transmission electron microscopy. Dentin remineralization was best achieved using MTA containing biomimetic analogs regardless of whether an adhesive was applied; dentinal tubules within the remineralized dentin were occluded by apatite. It is concluded that the version of MTA employed in this study may be doped with biomimetic analogs for remineralization of unbonded and bonded artificial caries-like lesions in the presence of SBF.

1. Introduction

Minimally invasive treatment of deep dentin caries adjacent to vital pulps has been used in attempts to preserve caries-affected and even caries-infected dentin [1,2]. As caries is a dynamic process caused by an imbalance between demineralization and remineralization, fluoride-releasing restorative materials are used to restore the imbalance [3,4]. Although fluoride is not considered a common feature in naturally occurring biomineralization [5], its beneficial effects on enamel remineralization cannot be overstated. This applies especially to the improved dissolution resistance initiated by epitaxial deposition of fluorapatite over remnant apatite crystallites [6]. Nevertheless, remineralization of dentin with fluoride is more difficult to achieve than remineralization of enamel [7]. While there are numerous studies showing that dentin remineralization is enhanced in the presence of fluoride [8,9], remineralization was only observed on the surface of etched enamel, not on the surface of etched dentin under the same remineralizing conditions [10]. This may be attributed to the paucity of apatite seed crystallites available for heterogeneous crystal growth [11].

Extracellular matrix proteins play critical roles in controlling apatite nucleation and growth in collagenous tissues [12]. Polycarboxylic acid biomimetic analogs of matrix proteins participate in recruitment of pre-nucleation clusters [13] to produce fluidic, polymer-stabilized amorphous calcium phosphate nanoprecursors [14]. These fluidic nanoprecursors infiltrate collagen fibrils and transform into intrafibrillar apatite using the fibrils as biomineralization templates [15]. Polyphosphates play an important role in the biomineralization of apatite [16]. Using polyacrylic acid and sodium tripolyphosphate as dual biomimetic analogs of matrix proteins, intrafibrillar apatite platelets were deposited in an ordered manner within collagen fibrils [17,18]. These results suggest that fluoride-free remineralization of the apatite-sparse surface of completely demineralized dentin may be achieved with biomimetic

* Corresponding authors. Tel.: +86 20 83862558; fax: +86 20 83870412 (J.-Q. Ling), tel.: +1 706 721 2031; fax: +1 706 721 6252 (F.R. Tay).
E-mail addresses: lingjq@mail.sysu.edu.cn (J.-Q. Ling), ftay@georgiahealth.edu, tayfranklin7@gmail.com (F.R. Tay).
[1] Equal contributors.

1742-7061/$ - see front matter © 2011 Acta Materialia Inc. Published by Elsevier Ltd. All rights reserved.
doi:10.1016/j.actbio.2011.10.033

analogs of matrix proteins to overcome the thermodynamic energy barrier associated with homogeneous crystal nucleation [19].

Mineral trioxide aggregate (MTA) has found important applications in dentistry due to its biocompatibility and bioactive properties [20–22], among which is direct pulp capping [23]. The generic label "MTA" has been adopted for the different versions of mineral trioxide aggregate that are commercially available from different countries of origin. As the calcium silicate-containing material lacks phosphate, MTA becomes bioactive and produces apatite only when it comes into contact with phosphate-containing fluids [24–26]. Pulp-capping materials are often applied on caries-affected dentin. As indirect and direct pulp capping involves contact of restorative materials with phosphate-containing body fluids, calcium silicate-containing materials may be potentially employed for remineralization of dentinal caries in vital teeth. Although not currently included in its repertoire of clinical applications [23], it is envisaged that MTA may be modified for caries remineralization. Biomimetic mineralization of caries-like lesions has recently been reported with the use of Portland cement in the presence of polyacrylic acid and polyvinylphosphonic acid-containing simulated body fluid (SBF) [27] or polyacrylic acid and sodium tripolyphosphate-containing SBF [28]. While these studies provide the proof-of-concept that the procedure is an effective in vitro approach to more optimal remineralization of the mineral-sparse surface of a carious lesion, it is not possible to rely on dissolving biomimetic analogs in body fluids in a clinical setting. This necessitates the development of alternative approaches to translate the biomimetic remineralization strategy into a clinical delivery system. Moreover, Portland cement is not acceptable for clinical use due to its lack of radiopacity or the inclusion of potentially cytotoxic mineral elements [29]. Thus, the purpose of the present study was to determine if biomimetic analogs may be incorporated in MTA, a clinically acceptable, radiopaque Portland cement-based material for remineralization of artificial caries-like dentin. Specifically, as dentin remineralization with calcium phosphate resin cements is adversely affected by dentin adhesive application [30], the effects of dentin remineralization with biomimetic analogs-incorporated MTA in the presence or absence of dentin bonding were evaluated. The null hypothesis tested was that the dentin remineralization efficacy of MTA in SBF is not affected by the incorporation of biomimetic analogs or adhesive application.

2. Materials and methods

2.1. Preparation of artificial dentin caries lesions

Forty non-carious human third molars were obtained under a protocol approved by the Human Assurance Committee of the Georgia Health Sciences University. A 1 mm thick disk devoid of pulp exposure and remnant enamel over the surface of the exposed occlusal dentin was prepared perpendicular to the longitudinal axis of each tooth using a low-speed Isomet saw (Buehler, Lake Bluff, IL) under water cooling. The surface for creating the caries-like lesion was polished with 1200-grit silicon carbide paper to create a smooth surface. The opposing surface, together with the enamel rim and 1 mm of peripheral dentin of the polished surface (to serve as reference), was protected with varnish to limit the areas available for demineralization. A 280 ± 20 μm thick layer of partially demineralized dentin was created on the uncoated surface by pH cycling [31]. The demineralizing solution consisted of 1.5 mM $CaCl_2$, 0.9 mM KH_2PO_4, 50 mM acetic acid and 5 mM NaN_3 adjusted to pH 4.8. The remineralizing solution consisted of 1.5 mM $CaCl_2$, 0.9 mM NaH_2PO_4, 0.13 M KCl and 5 mM NaN_3 adjusted to pH 7.0 with HEPES buffer. Each specimen was immersed in 10 ml of the demineralizing solution for 8 h followed by immersion in 10 ml of the remineralizing solution for 16 h, with new solutions used for each cycle. This procedure was performed for 14 days at ambient temperature.

2.2. Microcomputed tomography

After pH cycling, each disk was sectioned to create a 4 mm wide slab containing the caries-like lesion. Each lesion was characterized non-destructively by microcomputed tomography using the method reported by Liu et al. [27] to determine the lesion depth and integrated mineral loss (ΔZ) across the entire 4 mm wide lesion. Briefly, the mineral profile of each artificial caries-like lesion was scanned under water using a SkyScan 1174 scanner (Micro Photonics, Allentown, PA, USA). A positioning jig was prepared for each specimen from a sectioned pipette tip. Low-viscosity polyvinylsiloxane impression material was injected into a sectioned pipette tip followed by insertion of a dentin slab to produce a slotted mold in which the slab could be covered with water during scanning (Fig. 1A). Precise fitting of the slab into the slotted mold enabled it to be removed from the jig for mineralization and to be reinserted into the same position for multiple microcomputed tomography scans. A 1 mm thick aluminum filter was placed in front of the detector to remove low-energy radiation from the polychromatic X-ray source. Scanning was performed with a spatial resolution of 6.28 μm. Projection images were collected at 50 kV and 800 μA using 360° rotation, with 3 s exposure time per 0.6° projection step. Signal-to-noise ratio was improved by averaging of 30 frames. During the reconstruction phase using the NRecon software (Version 1.6.2), a 20% beam hardening correction was employed to reduce ring artifacts. After image reconstruction, two-dimensional (2-D) slices in the sagittal plane were acquired using Data Viewer and saved in a 256 grayscale format. The same parameters were used when the same slab was re-scanned during subsequent months.

Sagittal virtual serial sections derived from each slab were used to create a 2-D stacked image with CTAnalyzer. The stacked 2-D image was imported into ImageJ (NIH, Bethesda, MD, USA) to produce an overall mineral profile within a standardized volume of interest (VOI). A white vertical line was formed extending from the radiopaque, non-demineralized part of the slab surface to the radiolucent surface of the artificial carious lesion (Fig. 1B). This virtual line served as the superimposition reference for mineral

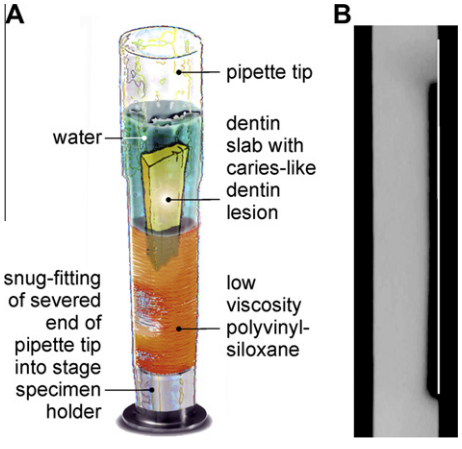

Fig. 1. Schematics of the methods employed in microcomputed tomography of artificial caries-like lesions. (A) Design of a specimen-specific positioning jig for repeated scanning of an artificial caries-like lesion under water to prevent dehydration during scanning. (B) Placement of a virtual line over the surface of a stacked image derived from multiple virtual sections obtained from microcomputed tomography for evaluation of the lesion depth and integrated mineral loss.

profiles obtained during different time periods and eliminated streak artifacts that were created by a polychromatic X-ray source when a high attenuation object is placed adjacent to the VOI [32]. A rectangular area function was used to capture the grayscale attenuation value distribution across the sagittal plane of a selected area within the stacked image. The VOI for all specimens consisted of a 4 mm long × 1 mm wide area within the sagittal plane. Lengthwise, the rectangular area commenced from 0.5 mm below the non-demineralized slab surface and included only the artificial carious lesion. Widthwise, the rectangular area extended from 0.2 mm external to the virtual reference line into the unaltered mineralized tissue. The same scaling parameters were applied to all stacked images that were subsequently obtained from each specimen.

The length scale of the ordinate in the overall mineral profile was expressed in micrometers. Mineral profiles were measured from the lesion surface to the point where the relative mineral content was 95% of the underlying mineralized dentin base [33]. Grayscale attenuation values in the abscissa were expressed as the relative mineral volume by normalizing the mineral density of the unaltered dentin to 50 vol.% mineral density [34,35]. The lesion depth (μm) and the integrated mineral loss (ΔZ) from the artificial carious lesion (μm vol.%) were recorded as baseline data for evaluating the remineralization efficacy.

2.3. Remineralization protocols

The caries-like lesions were distributed into four groups ($n = 10$). Slab assignments were analyzed with one-way analysis of variance (ANOVA) to ensure that there were no differences in the baseline lesion depth and ΔZ values among the four groups. An experimental pre-marketed version of white MTA (MTA Plus™, Prevest Denpro, Jammu City, India) was used as the calcium and hydroxyl ion-releasing source. This material has a finer particle size than other commercially available versions (50% of the particles finer than 1 μm; C.M. Primus, unpublished results) and utilizes a proprietary salt-free polymer gel in place of water as the mixing vehicle to improve its washout resistance. The material was mixed using a 3:1 powder-liquid ratio to achieve a putty-like consistency, with a setting time of 1.2 h. The mixed material was placed into 4 × 8 × 2 mm silicone molds and allowed to set completely at 37 °C and 100% relative humidity before use.

To examine the effect of the first factor "protocol" on remineralization efficacy, set MTA was used for two groups that were designated as "control". For the other two groups, designated as "biomimetic", the MTA was first mixed into a putty-like consistency. A mixture of 3 wt.% polyacrylic acid powder ($M_w = 1800$; Sigma–Aldrich, St. Louis, MO) and 8 wt.% sodium tripolyphosphate powder ($M_w = 367.8$; Sigma–Aldrich) was used as biomimetic analogs of dentin matrix proteins [18]. The powder was blended with the mixed MTA and allowed to set under similar conditions.

To examine the effect of the second factor "adhesive application" on remineralization efficacy, two groups were designated as "no adhesive", with the caries-like lesions remineralized as prepared. For both the adhesive experimental group and its corresponding control group, two coats of an acetone-based unfilled adhesive (One-Step, Bisco Inc., Schaumburg, IL) were liberally applied to the artificial dentinal carious lesion, then light-polymerized for 20 s. As the lesions were already partially demineralized, no additional phosphoric acid etchant was employed prior to the application of the two-step etch-and-rinse adhesive. Thus, evaluation of the combined effects of "protocol" and "adhesive application" resulted in an experimental design with four groups: (1) control–adhesive, (2) control–no adhesive, (3) biomimetic–adhesive and (4) biomimetic–no adhesive.

2.4. Remineralization of caries-like lesions

SBF (pH adjusted to 7.4) was prepared as the phosphate source by dissolving 136.8 mM NaCl, 4.2 mM $NaHCO_3$, 3.0 mM KCl, 1.0 mM $K_2HPO_4{\cdot}3H_2O$, 1.5 mM $MgCl_2{\cdot}6H_2O$, 2.5 mM $CaCl_2$ and 0.5 mM Na_2SO_4 in deionized water and adding 3.08 mM sodium azide to prevent bacterial growth. For each caries-like lesion, the set MTA block prepared for the designated group was placed on the lesion surface to simulate placement of a capping material over an unbonded or bonded lesion. Each dentin slab was placed inside a glass scintillation vial with the surface of the partially demineralized slab in contact with a set MTA block. The vial was filled with 10 ml of SBF and incubated at 37 °C, with changes in the SBF every 2 days. Each dentin slab was retrieved at designated time intervals (2, 4 and 6 weeks), inserted in the positioning jig prepared specifically for that specimen and scanned under water to prevent dehydration shrinkage. After scanning, the dentin slab was returned to the corresponding vial to continue remineralization.

2.5. Statistical analyses

Remineralization data obtained after 6 weeks were analyzed for their normality (Shapiro–Wilk test) and equal variance (Levene test) assumptions to determine the feasibility of using parametric statistical methods. Accordingly, two-way ANOVA and Holm–Sidak multiple comparisons were employed to examine the effects of "protocol" and "adhesive application", and the interaction of these two factors, on lesion depth reduction. The overall remineralization efficacy ($(\Delta Z_{baseline} - \Delta Z_{6\ weeks})/\Delta Z_{baseline} \times 100\%$) was analyzed with Kruskal–Wallis ANOVA and Dunn's multiple comparisons. Statistical significance for all procedures was preset at $\alpha = 0.05$.

2.6. Transmission electron microscopy (TEM)

After 6 weeks of remineralization, four representative specimens from each group were fixed in Karnovsky's fixative, post-fixed with 1% osmium tetroxide, dehydrated in an ascending ethanol series (30–100%), transitioned through propylene oxide and embedded in epoxy resin. Baseline lesions were similarly prepared. Thick sections (180–200 nm) of the caries-like lesion including the mineralized dentin base were prepared without additional demineralization and examined unstained for evaluating the overall effect of remineralization. Resin blocks were then trimmed for thin section preparation (90 nm). Examination was performed using a JEM-1230 transmission electron microscope (JEOL, Tokyo, Japan) at 110 kV. Selected area electron diffraction was used for characterization of the remineralized mineral phase.

3. Results

There were no significant differences ($p > 0.05$) in the baseline mineral profiles (designated by "a") among the four groups (Table 1). For lesion depth, remineralization was significantly affected by "protocol" ($p < 0.001$) and "adhesive application" ($p < 0.001$); the interaction of those two factors was not significant ($p = 0.489$). Reduction in lesion depths followed the order: biomimetic–no adhesive "e" > biomimetic–adhesive "d" > control–no adhesive "c" > control–adhesive "b". Statistical analysis showed that the overall remineralization efficacies of the control groups "b" and "c" were not significantly different but were significantly lower ($p < 0.05$) than the biomimetic groups "d" and "e", which, in turn, were not significantly different from each other. Representative mineral profiles of baseline and remineralized lesions at 6 weeks are shown in Fig. 2A. Changes in mineral profiles over the 6 week

Table 1
Changes in lesion depth and integrated mineral loss (ΔZ) from partially demineralized artificial caries-like lesions following remineralization with MTA in the presence or absence of biomimetic analogs.

Parameter	Time period	"b" Control[†]–adhesive (n = 10)	"c" Control[†]–no adhesive (n = 10)	"d" Biomimetic[‡]–adhesive (n = 10)	"e" Biomimetic[‡]–no adhesive (n = 10)
Lesion depth (μm)	"a" Baseline[*]	286.0 ± 16.6^{x}	279.1 ± 7.3^{x}	280.4 ± 14.0^{x}	288.5 ± 17.8^{x}
	2 weeks	272.2 ± 7.7	250.7 ± 16.2	165.1 ± 16.5	146.1 ± 10.2
	4 weeks	253.9 ± 32.0	237.5 ± 20.8	143.0 ± 14.6	75.6 ± 14.6
	6 weeks[**]	231.8 ± 36.7^{A,1}	206.0 ± 10.7^{A,2}	106.5 ± 14.1^{B,1}	69.5 ± 30.1^{B,2}
ΔZ (μm vol.%)	"a" Baseline[*]	4923.5 ± 283.8^{Y}	4908.2 ± 130.0^{Y}	4943.3 ± 220.0^{Y}	4732.4 ± 240.3^{Y}
	2 weeks	4647.4 ± 347.9	4526.4 ± 400.9	2565.0 ± 146.7	1631.1 ± 224.9
	4 weeks	4555.5 ± 399.6	3779.6 ± 220.2	808.6 ± 138.2	358.7 ± 124.9
	6 weeks	4354.7 ± 303.4	3563.7 ± 328.0	554.5 ± 164.8	213.4 ± 177.7
Remineralization efficacy at 6 weeks[***]		11.9 ± 7.2^{a}	27.3 ± 7.4^{a}	88.7 ± 3.5^{b}	98.5 ± 0.6^{b}

"a", "b", "c", "d" and "e" correspond to the designations adopted for Figs. 2–4. Values are means ± standard deviations.
[†] Control: remineralization with MTA only in SBF.
[‡] Biomimetic: remineralization with biomimetic analogs-containing MTA in SBF.
[*] For each parameter (lesion depth or ΔZ), values with the same upper letter superscript are not statistically significant ($p > 0.05$).
[**] The first letter superscript represents "control" vs. "biomimetic" remineralization; values with different superscript letters are statistically significant ($p < 0.05$). The second numeral superscript represents "adhesive" vs. "no adhesive". Values with different numerical superscripts are statistically significant ($p < 0.05$).
[***] Remineralization efficacy = $((\Delta Z_{baseline} - \Delta Z_{6\ weeks})/\Delta Z_{baseline} \times 100\%)$, where ΔZ represents the integrated mineral loss from the artificial caries-like dentin. Values with different lower letter superscripts are statistically significant ($p < 0.05$).

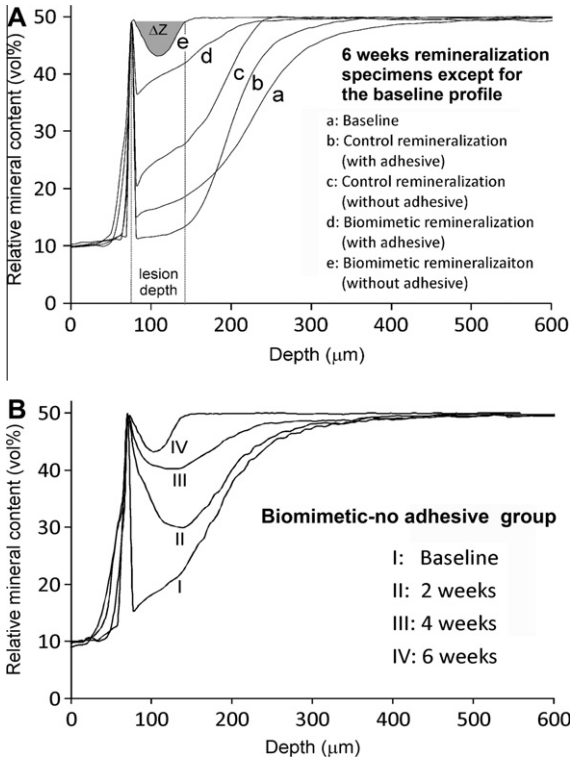

Fig. 2. (A) Representative examples of the mineral profiles of the baseline artificial caries-like lesion "a" and the four remineralized groups after 6 weeks "b–e". Lesion depth and integrated mineral loss (ΔZ) are illustrated for "e". Apart from being the most highly mineralized, "e" is different in that the surface of the lesion was more heavily remineralized than the subsurface due to occlusion of the dentinal tubules with mineral plugs (see Fig. 4E and F). (B) Changes in mineral profile from a representative specimen in the biomimetic–no adhesive group "e" over a 6 week remineralization period.

period are illustrated by a representative specimen from the biomimetic–no adhesive group "e" (Fig. 2B).

Representative images from unstained thick sections of baseline and remineralized lesions are shown in Fig. 3. Fig. 3a represents a baseline artificial caries-like lesion with an approximately 300 μm thick zone of partially demineralized dentin that exhibited a gradient of increasing mineral density from the lesion surface to the base of the lesion. Fig. 3b represents the results of remineralization of an adhesive-bonded lesion for 6 weeks in the absence of biomimetic analogs (control–adhesive). There was little change in the electron density of the lesion compared with the baseline, non-remineralized lesion. Fig. 3c represents remineralization of an unbonded lesion for 6 weeks in the absence of biomimetic analogs (control–no adhesive). Although there was an overall increase in the mineral density of the subsurface part of the lesion, the lesion surface remained poorly remineralized. Fig. 3d represents remineralization of an adhesive-bonded lesion for 6 weeks in the presence of mixed-in biomimetic analogs in the MTA (biomimetic–adhesive). An increase in electron density of the surface part of the lesion can be seen, compared to the "control–adhesive" lesion in Fig. 3b. The lack of complete remineralization of the surface part of the lesion was due to filling of the interfibrillar spaces of that part of the partially demineralized collagen matrix with polymerized adhesive resin. Fig. 3e represents remineralization of an unbonded lesion for 6 weeks in the presence of mixed-in biomimetic analogs in the MTA (biomimetic–no adhesive). The overall electron density of the remineralized lesion was not visibly different from that of the underlying dentin base.

Unstained thin section images of the surface of a baseline lesion (Fig. 4A) and a lesion from the control–adhesive group "b" (Fig. 4B) showed sparsely distributed minerals in the intertubular dentin and dentinal tubules devoid of peritubular dentin. Surface remineralization was better achieved in the control–no adhesive group "c" (Fig. 4C) in the form of needle-shaped crystallites (Fig. 5A). Much denser surface remineralization was observed in the biomimetic–adhesive group "d", with dentinal tubules containing little intratubular mineral deposits (Fig. 4D). Heavy remineralization of the intertubular dentin was similarly seen in the biomimetic–no adhesive group "e" (Fig. 4E). Dentinal tubules along the top 30–40 μm of the lesion were occluded by apatite deposits (Fig. 4F). Electron-dense mineral platelets could be identified from the biomimetically remineralized lesion (Fig. 5B). Tubular occlusion was confirmed from all specimens derived from this group. Volume renderings of a baseline lesion and a lesion remineralized

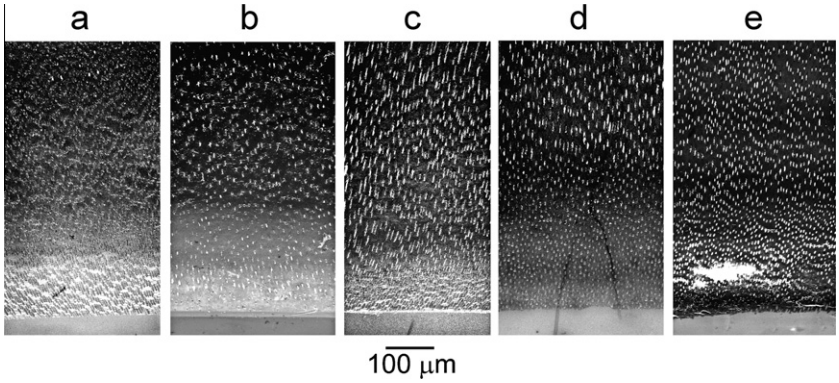

Fig. 3. TEM images of thick unstained sections prepared from representative examples of: "a" a baseline artificial caries-like lesion before remineralization; "b" an adhesive-bonded lesion remineralized in MTA Plus™ and SBF (control–adhesive) after 6 weeks; "c" control remineralization of an unbonded lesion after 6 weeks (control–no adhesive); "d" an adhesive-bonded lesion remineralized in MTA Plus™ containing mixed-in biomimetic analogs and SBF (biomimetic–adhesive) after 6 weeks; "e" biomimetic remineralization of an unbonded lesion after 6 weeks (biomimetic–no adhesive). The tear in the section was caused by incomplete epoxy resin infiltration.

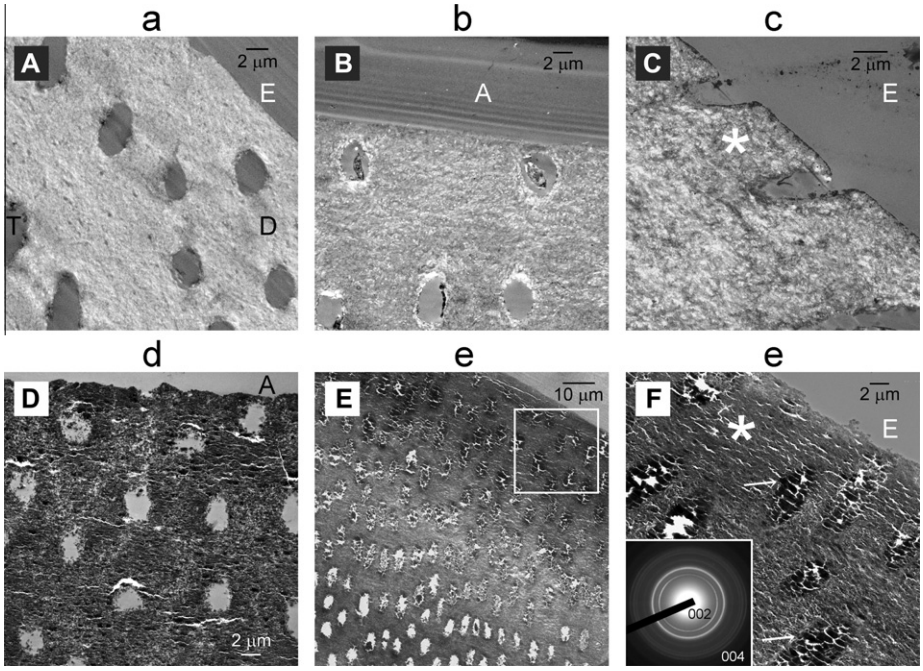

Fig. 4. TEM images prepared from unstained thin sections of representative examples remineralized for 6 weeks illustrating the extent of remineralization along the lesion surface. The lowercase letter at the top of each image corresponds to the group designation in Figs. 2 and 3. D: intertubular dentin; T: dentinal tubules from the surface of the artificial caries-like lesion were devoid of peritubular dentin; A: dentin adhesive; E: epoxy resin. For the biomimetic–no adhesive group "e" (E), dentinal tubules within the surface 50 μm of the remineralized lesion were occluded by minerals. Higher magnification of the region demarcated by the white box (F) shows heavy occlusion of dentinal tubules (arrows) by apatite deposits, as indicated by selected area electron diffraction (inset).

with the biomimetic–no adhesive protocol are illustrated as Quicktime movies in the Appendix I.

4. Discussion

The results warrant rejection of the null hypothesis that the dentin remineralization efficacy of MTA in SBF is not affected by the incorporation of biomimetic analogs or adhesive application. In the present study, unset MTA was not applied directly over the caries-like lesions for three reasons: (i) the block could be removed prior to microcomputed tomography scanning to prevent generation of streak artifacts by highly radiopaque materials; (ii) the procedure prevented tearing of non-remineralized collagen matrices during ultramicrotomy as the diamond knife cut through the MTA particles into the caries-like lesion; and (iii) it prevented any tubular occlusion by MTA particles that could have blocked subsequent observation of calcium phosphate deposits within the tubular orifices by TEM.

We did not measure mineral content by transverse microradiography [36] as MTA fractured from the dentin during the preparation of the thin slices. The method was also unsuitable for repeated measurements. However, we adopted the procedure employed in transverse microradiography by normalizing grayscale attenuation values derived from microcomputed tomography to the mineral density of unaltered dentin. As the attenuation values were not converted into "exact" mineral densities based on phantom calibrations [37,38], the data in the present study only represent relative mineral volumes.

Although microcomputed tomography was employed in the present study, it must be pointed out that other non-destructive evaluation techniques are also available. Quantitative

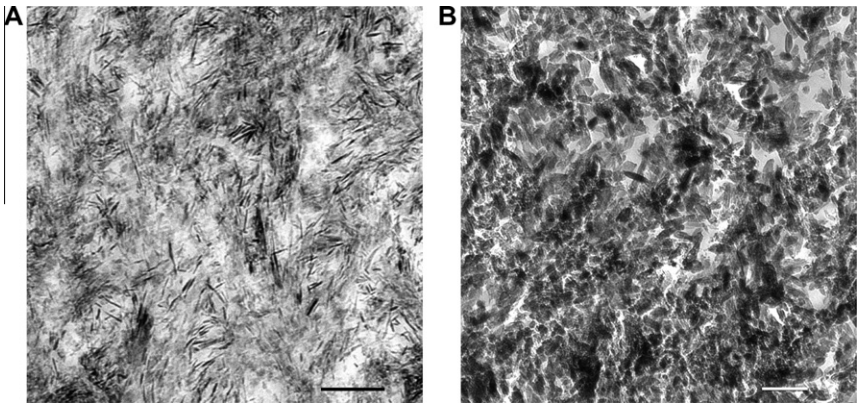

Fig. 5. High magnification unstained TEM images of crystallites present from the lesion surface remineralized for 6 weeks from (A) control remineralization groups (bar = 200 nm). The asterisk in Fig. 4C represents the location from which this image was taken. (B) Biomimetic remineralization groups (bar = 200 nm). The asterisk in Fig. 4F represents the location from which this image was taken.

light-induced fluorescence [39] and terahertz pulsed imaging [40], while useful for detecting incipient enamel caries, have not been optimally developed for evaluating carious dentin lesions. Polarization-sensitive optical coherence tomography (PS-OCT) is a promising non-destructive technique based on integrated reflectivity measurements [41]. Nevertheless, the axial resolution in PS-OCT is 16 μm in dentin compared with the 6.28 μm resolution obtained with the present scanner. In vitro PS-OCT evaluation of demineralized dentin also requires compensation for dehydration shrinkage that alters reflectivity readings [42]. By contrast, compensation is not required in the present study because the scanning of the partially demineralized dentin slabs was performed under water (Fig. 1A).

The overall improved remineralization efficacy associated with the biomimetic remineralization protocol may be partially attributed to the release of biomimetic analogs from set MTA. Although there is no reported method for spectrophotometric determination of the release of the polycarboxylic acid analog, there was a continuous release of the sodium tripolyphosphate analog from the set MTA blocks during the 6 week period, as determined by spectrophotometric estimation of the phosphate content with an ammonium molybdate assay based on analysis of the colored phosphomolybdate complex at 820 nm [43] (Appendix II). According to the non-classical crystallization theory [44], polycarboxylic acid analogs are capable of stabilizing amorphous calcium phosphates (ACPs) as liquid-like nanoprecursors [14], enabling them to self-assemble within the gap zones of collagen molecules and transform into apatite crystallites. The original intention of incorporating polyphosphate as the second biomimetic analog was based on our previous results that inclusion of phosphoprotein analogs in a biomineralization medium produced the ordered arrangement of intrafibrillar apatite platelets [17]. Nevertheless, release of polyphosphate from set MTA may also contribute to the improved remineralization efficacy in the biomimetic groups, which has to be confirmed in future studies. Inclusion of polyphosphate in the MTA may serve as a supplementary phosphate source when its availability is compromised beneath a restoration in non-vital teeth. Ongoing work is being carried out by incorporating tricalcium phosphate nanoparticulate powder in the mixed MTA for enhanced release of phosphate so that the biomimetic remineralization delivery system may be used in non-vital teeth. Pretreatment of the dentin lesions with a phosphate-containing solution or gel would be another option.

In the present study, no significant differences between the "adhesive" and "no adhesive" groups were apparent when their overall remineralization efficacies were analyzed using nonparametric statistical methods. We speculate that this may be caused by the small dimensions of calcium phosphate nucleation clusters. [13] As the CaP pre-nucleation clusters are ~1 nm in diameter, which is the approximate size of a Posner cluster (smallest structural unit of ACP), they can readily infiltrate the hydrophilic domains [45] or water channels [46] present within a polymerized hydrophilic adhesive.

It is pertinent to highlight that the remineralization kinetics observed in the present study (6 weeks) is faster than those reported in previous proof-of-concept studies when the biomimetic analogs were dissolved in SBF (3 months) [27]. This may be attributed to the close proximity of the biomimetic analogs with the artificial caries-like lesions. Moreover, degradation of the demineralized collagen matrices from the surface of the remineralized artificial caries-like lesions by endogenous matrix metalloproteinases present in dentin [28] was not observed in the present study as a result of the improved remineralization kinetics. This phenomenon has previously been observed using the proof-on-concept biomimetic remineralization strategy [47] and mimics the tubular occlusion observed in carious dentin [48]. As the experimental protocol involved placement of set MTA over the dentin lesion, such a phenomenon could not have been caused by the introduction of fine MTA particles into the dentinal tubules but represents genuine intratubular apatite deposits. Although tubular occlusion may hamper complete remineralization of the lesion surface, it is beneficial in reducing dentin hypersensitivity when the technique is used on actively progressing caries wherein the dentinal tubules are not completely occluded by whitlockite deposits.

It is of clinical relevance to examine if the MTA-based biomimetic remineralization protocol is applicable to genuine dentin carious lesions. These lesions should be more difficult to remineralize due to their variability in lesion depths and degrees of tubular occlusion [49]. Moreover, unlike artificial caries-like lesions, demineralization in genuine caries-affected dentin is often manifested as sporadic islands of demineralization instead of a continuous demineralization gradient from the lesion surface to the lesion base [50]. Further work should also be performed to address whether the mechanical properties of MTA are affected by the incorporation of biomimetic analogs, and to identify the most optimal means for delivery of these components to improve the kinetics of dentin remineralization.

5. Conclusion

Within the limits of the present study, it is concluded that the present version of MTA may be doped with biomimetic analogs for remineralization of unbonded and adhesive-bonded artificial caries-like lesions in the presence of SBF. Incorporation of biomi-

metic analogs in modified MTA provides a potential delivery system for realization of the goal of biomimetic remineralization of dentin and widens the scope of MTA applications in dentistry.

Acknowledgements

The authors acknowledge support from the National Institutes of Health (NIDCR R21 DE019213; PI Tay; NIDCR R01 DE015306; PI Pashley) and the PSRP and ESA awards from the Georgia Health Sciences University. C.M.P. declares potential conflict of interest as the inventor of white MTA and MTA Plus. The other authors declare no potential conflicts of interest with respect to the authorship and/or publication of this article. We thank Prevest Denpro for providing the MTA Plus™ and M. Burnside for secretarial support.

Appendix A. Supplementary data

Supplementary data associated with this article can be found, in the online version, at doi:10.1016/j.actbio.2011.10.033.

Appendix B. Figures with essential colour discrimination

Certain figure in this article, particularly Figure 1, is difficult to interpret in black and white. The full colour images can be found in the on-line version, at doi:10.1016/j.actbio.2011.10.033.

References

[1] Thompson V, Craig RG, Curro FA, Green WS, Ship JA. Treatment of deep carious lesions by complete excavation or partial removal: a critical review. J Am Dent Assoc 2008;139:705–12.
[2] Kidd EA. Clinical threshold for carious tissue removal. Dent Clin North Am 2010;54:541–9.
[3] Wiegand A, Buchalla W, Attin T. Review on fluoride-releasing restorative materials – fluoride release and uptake characteristics, antibacterial activity and influence on caries formation. Dent Mater 2007;23:343–62.
[4] Peters MC, Bresciani E, Barata TJ, Fagundes TC, Navarro RL, Navarro MF, et al. In vivo dentin remineralization by calcium-phosphate cement. J Dent Res 2010;89:286–91.
[5] Weiner S. Biomineralization: a structural perspective. J Struct Biol 2008;163:229–34.
[6] Featherstone JD. Caries prevention and reversal based on the caries balance. Pediatr Dent 2006;28:128–32.
[7] Damen JJ, Buijs MJ, ten Cate JM. Fluoride-dependent formation of mineralized layers in bovine dentin during demineralization in vitro. Caries Res 1998;32:435–40.
[8] Heilman JR, Jordan TH, Warwick R, Wefel JS. Remineralization of root surfaces demineralized in solutions of differing fluoride levels. Caries Res 1997;31:423–8.
[9] Preston KP, Smith PW, Higham SM. The influence of varying fluoride concentrations on in vitro remineralisation of artificial dentinal lesions with differing lesion morphologies. Arch Oral Biol 2008;53:20–6.
[10] Fan Y, Sun Z, Moradian-Oldak J. Controlled remineralization of enamel in the presence of amelogenin and fluoride. Biomaterials 2009;30:478–83.
[11] Liu Y, Sethuraman G, Wu W, Nancollas GH, Grynpas M. The crystallization of fluorapatite in the presence of hydroxyapatite seeds and of hydroxyapatite in the presence of fluorapatite seeds. J Colloid Interface Sci 1997;186:102–9.
[12] George A, Veis A. Phosphorylated proteins and control over apatite nucleation, crystal growth, and inhibition. Chem Rev 2008;108:4670–93.
[13] Dey A, Bomans PH, Müller FA, Will J, Frederik PM, de With G, et al. The role of prenucleation clusters in surface-induced calcium phosphate crystallization. Nat Mater 2010;9:1010–4.
[14] Gower LB. Biomimetic model systems for investigating the amorphous precursor pathway and its role in biomineralization. Chem Rev 2008;108:4551–627.
[15] Nudelman F, Pieterse K, George A, Bomans PH, Friedrich H, Brylka LJ, et al. The role of collagen in bone apatite formation in the presence of hydroxyapatite nucleation inhibitors. Nat Mater 2010;9:1004–9.
[16] Omelon SJ, Brynpas MD. Relationships between polyphosphate chemistry, biochemistry and apatite biomineralization. Chem Rev 2008;108:4694–715.
[17] Liu Y, Kim YK, Dai L, Li N, Khan SO, Pashley DH, et al. Hierarchical and non-hierarchical mineralisation of collagen. Biomaterials 2011;32:1291–300.
[18] Liu Y, Li N, Qi YP, Dai L, Bryan TE, Mao J, et al. Intrafibrillar collagen mineralization produced by biomimetic hierarchical nanoapatite assembly. Adv Mater 2011;23:975–80.
[19] Wang L, Nancollas GH. Pathways to biomineralization and biodemineralization of calcium phosphates: the thermodynamic and kinetic controls. Dalton Trans 2009;15:2665–72.
[20] Camilleri J, Pitt Ford TR. Mineral trioxide aggregate: a review of the constituents and biological properties of the material. Int Endod J 2006;39:747–54.
[21] Parirokh M, Torabinejad M. Mineral trioxide aggregate: a comprehensive literature review. Part I. Chemical, physical, and antibacterial properties. J Endod 2010;36:16–27.
[22] Torabinejad M, Parirokh M. Mineral trioxide aggregate: a comprehensive literature review. Part II. Leakage and biocompatibility investigations. J Endod 2010;36:190–202.
[23] Parirokh M, Torabinejad M. Mineral trioxide aggregate: a comprehensive literature review. Part III. Clinical applications, drawbacks, and mechanism of action. J Endod 2010;36:400–13.
[24] Tay FR, Pashley DH, Rueggeberg FA, Loushine RJ, Weller RN. Calcium phosphate phase transformation produced by the interaction of the Portland cement component of white mineral trioxide aggregate with a phosphate-containing fluid. J Endod 2007;33:1347–51.
[25] Okiji T, Yoshiba K. Reparative dentinogenesis induced by mineral trioxide aggregate: a review from the biological and physicochemical points of view. Int J Dent 2009;464280.
[26] Darvell BW, Wu RC. "MTA" – an hydraulic silicate cement: review update and setting reaction. Dent Mater 2011;7:407–22.
[27] Liu Y, Mai S, Li N, Yiu CK, Mao J, Pashley DH, et al. Differences between top-down and bottom-up approaches in mineralizing thick, partially demineralized collagen scaffolds. Acta Biomater 2011;7:1742–51.
[28] Liu Y, Li N, Qi Y, Niu LN, Elshafiy S, Mao J, et al. The use of sodium trimetaphosphate as a biomimetic analog of matrix phosphoproteins for remineralization of artificial caries-like dentin. Dent Mater 2011;27:465–77.
[29] Tenório de Franca TR, da Silva RJ, Sedycias de Queiroz M, Aguiar CM. Arsenic content in Portland cement: a literature review. Indian J Dent Res 2010;21:591–5.
[30] Dickens SH, Flaim GM. Effect of a bonding agent on in vitro biochemical activities of remineralizing resin-based calcium phosphate cements. Dent Mater 2008;24:1273–80.
[31] ten Cate JM, Buijs MJ, Damen JJ. pH-cycling of enamel and dentin lesions in the presence of low concentrations of fluoride. Eur J Oral Sci 1995;103:362–7.
[32] De Man B, Nuyts J, Dupont P, Marchal G, Suetens P. Reduction of metal streak artifacts in X-ray computed tomography using a transmission maximum a posterior algorithm. IEEE Trans Nuclear Sci 2000;47:977–81.
[33] Gelhard TBFM, Arends J. Microradiography of in vivo remineralized lesions in human enamel. J Biol Buccale 1984;12:59–65.
[34] ten Cate JM, Damen JJ, Buijs MJ. Inhibition of dentin demineralization by fluoride in vitro. Caries Res 1998;32:141–7.
[35] Märten A, Fratzl P, Paris O, Zaslansky P. On the mineral in collagen of human crown dentine. Biomaterials 2010;31:5479–90.
[36] Ten Bosch JJ, Angmar-Månsson B. A review of quantitative methods for studies of mineral content of intra-oral incipient caries lesions. J Dent Res 1991;70:2–14.
[37] Zou W, Gao J, Jones AS, Hunter N, Swain MV. Characterization of a novel calibration method for mineral density determination of dentine by X-ray micro-tomography. Analyst 2009;134:72–9.
[38] Neves Ade A, Coutinho E, Vivan Cardoso M, Jaecques SV, Van Meerbeek B. Micro-CT based quantitative evaluation of caries excavation. Dent Mater 2010;26:579–88.
[39] Pretty IA, Smith PW, Edgar WM, Higham SM. Detection of in vitro demineralization adjacent to restorations using quantitative light induced fluorescence (QLF). Dent Mater 2003;19:368–74.
[40] Churchley D, Lynch RJ, Lippert F, Eder JS, Alton J, Gonzalez-Cabezas C. Terahertz pulsed imaging study to assess remineralization of artificial caries lesions. J Biomed Opt 2011;16:026001.
[41] Manesh SK, Darling CL, Fried D. Nondestructive assessment of dentin demineralization using polarization-sensitive optical coherence tomography after exposure to fluoride and laser irradiation. J Biomed Mater Res B Appl Biomater 2009;90:802–12.
[42] Lee C, Darling CL, Fried D. Polarization-sensitive optical coherence tomographic imaging of artificial demineralization on exposed surfaces of tooth roots. Dent Mater 2009;25:721–8.
[43] Chen PS, Toribara TY, Warner H. Microdetermination of phosphorus. Anal Chem 1956;28:1756–8.
[44] Cölfen H. Biomineralization: a crystal-clear view. Nat Mater 2010;9:960–1.
[45] Ye Q, Wang Y, Spencer P. Nanophase separation of polymers exposed to simulated bonding conditions. J Biomed Mater Res B Appl Biomater 2009;88:339–48.
[46] Tay FR, Pashley DH. Water treeing – a potential mechanism for degradation of dentin adhesives. Am J Dent 2003;16:6–12.
[47] Mai S, Kim YK, Kim J, Yiu CK, Ling J, Pashley DH, et al. In vitro remineralization of severely compromised bonded dentin. J Dent Res 2010;89:405–10.
[48] Zavgorodniy AV, Rohanizadeh R, Bulcock S, Swain MV. Ultrastructural observations and growth of occluding crystals in carious dentine. Acta Biomater 2008;4:1427–39.
[49] Pugach MK, Strother J, Darling CL, Fried D, Gansky SA, Marshall SJ, et al. Dentin caries zones: mineral, structure, and properties. J Dent Res 2009;88:71–6.
[50] Silva NR, Carvalho RM, Pegoraro LF, Tay FR, Thompson VP. Evaluation of a self-limiting concept in dentinal caries removal. J Dent Res 2006;85:282–6.